

# Effect of free carriers and impurities on the density of states and optical spectra of two-dimensional magnetoexcitons

Anna Gładysiewicz, Leszek Bryja, and Arkadiusz Wójs

*Institute of Physics, Wrocław University of Technology, Wybrzeże Wyspiańskiego 27, 50-370 Wrocław, Poland*

Marek Potemski

*Grenoble High Magnetic Field Laboratory, CNRS, F-38042 Grenoble Cedex 9, France*

(Received 13 June 2006; published 27 September 2006)

The density of states (DOS) and absorption spectrum of weakly doped, narrow quantum wells in high magnetic fields are calculated by realistic exact diagonalization. The systems containing an electron-hole pair with and without an additional second electron are compared. In the DOS, the exciton-electron interaction is shown to fill the gaps between Landau levels and to yield additional discrete peaks corresponding to bound trion states. In absorption, the interaction with the additional free electron causes no shift or renormalization of main excitonic peaks. However, it results in additional weaker peaks associated with bound trions in the lowest or higher Landau levels. The calculation is supplemented with experimental photoluminescence and photoluminescence-excitation studies of two-dimensional holes and electrons in high magnetic fields.

DOI: [10.1103/PhysRevB.74.115332](https://doi.org/10.1103/PhysRevB.74.115332)

PACS number(s): 71.35.Pq, 71.35.Ji, 71.10.Pm

## I. INTRODUCTION

Trions (also called charged excitons) are bound states of a neutral exciton (electron-hole pair,  $X=e+h$ ) with an additional carrier, either an electron or valence hole, for a negative ( $X^-=2e+h$ ) or positive ( $X^+=2h+e$ ) trion, respectively.<sup>1,2</sup> Neutral and charged excitons occur naturally in photoluminescence (PL) experiments, in which creation or annihilation of  $e-h$  pairs accompanies interband absorption or emission of light.<sup>3</sup> While excitons are expected in charge-neutral systems, the formation of trions depends on the presence of free carriers.

The trion binding energy  $\Delta$  is defined as the effective attraction between an exciton and an additional carrier ( $\Delta = E[X] + E[e] - E[X^\pm]$ , where  $E[\dots]$  is the ground energy of a given complex). An important material parameter affecting  $\Delta$  is the ratio of electron and hole effective masses,<sup>4</sup>  $\eta = \mu_e/\mu_h$ ; for  $\eta=0$  the  $X^-$  dynamics reduces to a familiar problem of the  $D^-$  center.<sup>5,6</sup> Originating from the charge-dipole interaction, trion binding is usually much weaker than exciton binding. However, its strong enhancement by spatial confinement and/or magnetic field  $B$  was predicted.<sup>7</sup> The pioneering experiment of Kheng *et al.*<sup>2</sup> in CdTe, followed by a series of measurements in GaAs (Refs. 8–11) and ZnSe (Refs. 12 and 13) confirmed that it is sufficient for trion detection. The  $X^+$  was also observed<sup>14,15</sup> and shown to be different from  $X^-$  (due to the  $\eta \leftrightarrow \eta^{-1}$  asymmetry).

In a typical experimental configuration, a quantum well containing a quasi-two-dimensional (quasi-2D) electron (or hole) gas is placed in the perpendicular field. The field should be sufficiently strong to induce magnetic quantization of single-particle states into macroscopically degenerate Landau levels (LL's), with the inter-LL (cyclotron) spacing  $\hbar\omega_c$  which is at least comparable to the effective excitonic Rydberg number ( $N_{Ry} \approx 5.5$  meV in GaAs). The well width  $w$  should not be much greater than the effective excitonic Bohr radius ( $a_B \approx 10$  nm in GaAs) and the magnetic length ( $\lambda = \sqrt{\hbar c/eB} \approx 8.1$  nm at  $B=10$  T).

The quantum-mechanical problem of a 2D exciton in a high magnetic field goes back several decades.<sup>16–18</sup> The continuous (owing to the neutral charge) energy dispersion in some idealized situations is known analytically, and the deviations due to inter-LL mixing or finite well width have been studied experimentally and numerically.<sup>19</sup> The simple  $q=0$  optical selection rule ( $q$  being the wave vector of an annihilated  $e-h$  pair) results from the small momentum carried by the absorbed or emitted photon. In experiment, the excitonic recombination is usually observed in the PL of quantum wells containing no free carriers.

Two-dimensional trions at high  $B$  have also been extensively studied in the past.<sup>20</sup> Different theoretical and computational approaches and the key results have been discussed in an exhaustive review by Peeters, Riva, and Varga.<sup>21</sup> Depending on the parameters (e.g.,  $w$  and  $B$ ), the trion energy spectrum contains one or more bound states, which can be conveniently labeled by the total spin  $S$  of the pair of electrons and total angular momentum  $M$ . At small  $B$ , the only bound  $X^-$  state is the spin singlet with  $S=0$  and  $M=0$ , equivalent to a 2D hydrogen ion.<sup>2,8–11</sup> In the (unrealistic) limit of very high  $B$  and vanishing  $w$ , the singlet unbinds and it is replaced by the spin-triplet with  $S=1$  and  $M=-1$ .<sup>22,23</sup> A triplet trion was identified by Shields *et al.*<sup>10</sup> (although now it is not clear if it was the  $M=-1$  triplet ground state). The singlet-triplet crossover was predicted<sup>24</sup> in rather high fields (e.g.,  $B \approx 30$  T in narrow symmetric GaAs wells). Despite initial difficulties<sup>25</sup> it was also eventually confirmed in several experiments.<sup>26–29</sup> Additional bound states were predicted<sup>30</sup> at intermediate  $B$ , but (for realistic parameters) they are always less strongly bound than the above two. These states were also confirmed by both independent calculations<sup>31</sup> and by experiments.<sup>27,28,32</sup>

The pair of optical selection rules results from invariance under (magnetic) translations<sup>33,34</sup> and from the particle-hole symmetry between conduction electrons and valence holes.<sup>35–37</sup> Both these “geometric” and “hidden” symmetries are at least weakly broken in realistic conditions. Neverthe-

less, recombination of trions with  $M \neq 0$  requires a symmetry-breaking collision (with an impurity or another carrier), and therefore, it became customary to label different trions as “bright” and “dark” (meaning having  $M=0$  and  $M \neq 0$ , respectively). In most recent experiments,<sup>25,27,32</sup> up to three trion states are observed: “bright” singlet  $X_s^-$ , “dark” triplet  $X_{td}^-$ , and a weakly bound “bright” triplet  $X_{tb}^-$  with  $S=1$  and  $M=0$ . The vanishing oscillator strength<sup>23,34</sup> of  $X_{td}^-$ , confirmed directly in optical absorption,<sup>38</sup> makes it more difficult to observe (even in PL) than the other trions. In fact, this state had not been conclusively identified until the work of Yusa *et al.*,<sup>27</sup> motivated by earlier high-field experiments (especially of Hayne *et al.*,<sup>25</sup> showing an apparent discrepancy with the prediction<sup>24</sup> of singlet-triplet crossing, but also several others<sup>26</sup> showing inconsistent features in trion spectra) and a numerical prediction<sup>30</sup> of an excited triplet state  $X_{tb}^-$ . Most recently, additional weakly bound states were reported<sup>29</sup> in CdTe ( $N_{Ry} \sim 10$  meV, about twice larger than in GaAs).

Involving only three particles, the trion’s quantum dynamics might appear to be relatively simple, both conceptually and computationally. The addition of a high magnetic field and confinement does not add much complexity, and indeed, quantum numbers and symmetries of all bound trions (in wide range of realistic conditions) are by now understood. In short, the dynamics depends on the competition of several energy scales, with the following characteristic values for our example of a 15-nm symmetric GaAs well at  $B=10$  T: cyclotron gap ( $\hbar\omega_c \sim 18$  meV for electrons and  $\sim 4$  meV for heavy holes), Coulomb energy ( $e^2/\lambda \sim 14$  meV), and a small Zeeman gap. The well width  $w$  comes in two places, defining excitation gaps to higher subbands (the gap to the second subband is  $\sim 50$  meV for electrons and  $\sim 10$  meV for holes) and affecting in-plane Coulomb matrix elements (this effect is parametrized by  $w/\lambda \sim 2$ ). Also, even weak asymmetry between electron and hole subband wave functions  $\chi_s(z)$  can considerably affect the trion binding, since it leads to different magnitudes of  $e-e$  and  $e-h$  interactions, which no longer cancel in  $\Delta$  (this effect is essential in asymmetric wells, not considered here, where the asymmetry depends on carrier concentration and/or additional gates).

However, the above optimistic (and popular) view hides the fact that a good understanding of the role of trions in PL experiments must include a variety of complications due to coupling to the environment (e.g., complex single-particle energy band structure with nonparabolic and anisotropic dispersions, interaction with free carriers, lattice defects, and phonons, spin-orbit effects, etc.). Some quantities (e.g., the binding energies, especially of the triplet states) can be calculated rather accurately.<sup>30,31</sup> However, others (such as the critical values of  $B$  and  $w$  for the singlet-triplet transitions) depend so sensitively on the (often unknown) parameters that their quantitative modeling turns out to be somewhat pointless. Another unsolved (quantitatively) and important problem is the kinetics of trions,<sup>39,40</sup> involving their binding and unbinding ( $X^- \leftrightarrow X + e^-$ ) and, at high  $B$ , orbital and spin relaxation ( $X_s^- \leftrightarrow X_{td}^- \leftrightarrow X_{tb}^-$ ).

In this article, we analyze the effect of trions on the optical absorption spectrum of 2D electrons in a magnetic field.

Thus, in addition to the earlier studied bound trion states,<sup>30,31</sup> the entire low-energy  $2e+h$  spectrum is considered. In a somewhat related work, the asymmetry of trion absorption peaks at small  $B$  was discussed by Stebe *et al.*<sup>41</sup> The inclusion of only two electrons and one hole in the model restricts it to the “dilute” regime, defined by a small value of the filling factor,  $\nu \ll 1$  ( $\nu$  is defined as the number of electrons  $N$  divided by the LL degeneracy  $g$ ; alternatively,  $\nu = 2\pi Q\lambda^2$  where  $Q$  is the 2D electron concentration). It is remarkable that in some systems the immersed trion is only weakly (perturbatively) affected by the surrounding electrons. In narrow wells and in high magnetic fields, this occurs at  $\nu < \frac{1}{3}$  due to “Laughlin correlations”<sup>42</sup> between electrons and trions,<sup>43</sup> preventing strong  $e-X^-$  collisions (indeed, in wider wells trions seem to be strongly coupled to the electrons and cannot be regarded as simple three-body quasiparticles<sup>44</sup>).

The density of states (DOS) and absorption spectra are calculated numerically by exact diagonalization in Haldane’s spherical geometry.<sup>45,46</sup> The figures were drawn for a particular choice of a symmetric  $w=15$  nm GaAs quantum well at  $B=10$  T. Since absorption into bound trion states was studied earlier, we concentrate on the effects of the interaction of the exciton with a (single) *unbound* electron. The main conclusions are a redistribution of the density of states (by filling the gaps between the LL’s) and the emergence of additional trion peaks in the absorption spectrum (also in the excited LL’s).

The calculation is supplemented with the results of experimental polarization-resolved PL and PL-excitation (PLE) studies of a 2D hole and electron gases in a symmetric 15-nm GaAs well. The presented spectra reveal absorption into a pair of bright trions in the lowest LL and emission from these two states: the exciton and the dark triplet trion.

## II. MODEL

The  $e+h$  and  $2e+h$  energy spectra are calculated by exact diagonalization of the Hamiltonian matrix on a Haldane sphere, convenient for modeling an infinite plane with 2D translational invariance. In this geometry, the magnetic field normal to the spherical surface of radius  $R$  is produced by a Dirac monopole of strength  $2Q=4\pi R^2 B/\phi_0$  ( $\phi_0 = hc/e$  is the magnetic flux quantum). Through the relation  $R^2 = Q\lambda^2$ , the monopole strength determines the surface curvature (in the magnetic units).

The single-particle states are called monopole harmonics.<sup>45</sup> They are the eigenstates of angular momentum  $l$  and its projection  $m$  on the  $z$  axis. The lowest shell, corresponding to the lowest LL, has  $l=Q$  and finite degeneracy  $g=2Q+1$ . Higher shells, corresponding to the excited LL’s labeled by index  $n$ , have  $l=Q+n$ .

The energy of the  $n$ th shell is  $\varepsilon_n = \hbar\omega_c(n + \frac{1}{2}) + \hbar^2 n(n+1)/2\mu R^2$ . It contains the cyclotron gap (with  $\omega_c = eB/\mu c$ , where  $\mu$  is the effective mass) and an additional curvature-dependent term. In order to model a real structure, we take advantage of the LL structure of monopole harmonics, but replace  $\varepsilon_n$  with the correct energies of electron and hole LL’s. E.g., at  $B=10$  T, we use  $\hbar\omega_c = 17.8$  meV for electrons

and 3.7 meV for the heavy hole (the latter value taken after Cole *et al.*<sup>47</sup> for  $w=15$  nm).

The second-quantization Hamiltonian reads

$$H = \sum_i c_i^\dagger c_i \varepsilon_i + \sum_{ijkl} c_i^\dagger c_j^\dagger c_k c_l v_{ijkl}. \quad (1)$$

An additional term  $\sum_{ij} c_i^\dagger c_j^\dagger c_l u_{ij}$  will also be included to describe the interaction with a positive or negative point charge. Here,  $c_i^\dagger$  and  $c_i$  are operators creating and annihilating a conduction electron or a valence hole in the state labeled by a composite index  $i$  containing all relevant single-particle quantum numbers (band  $\beta$ , subband  $s$ , LL index  $n$ , angular momentum  $m$ , and spin  $\sigma$ ).

The Coulomb interaction matrix elements  $v$  and  $u$  in the basis of monopole harmonics are known analytically for all particles confined to a 2D surface of the sphere. However, to account for a finite width of the real quantum well, we have integrated all matrix elements numerically, in 3D, using form factors appropriate for the actual electron and hole subband wave functions  $\chi_s(z)$ . Mixing with higher quantum well subbands (excited states in the  $z$  direction, labeled by  $s > 0$ ) is not very strong in a narrow and symmetric well due to high quantization energy (for  $w=15$  nm and  $\text{Al}_{0.35}\text{Ga}_{0.65}\text{As}$  barriers, it is 49.1 meV and 11.5 meV to the first excited electron and hole subbands, respectively; calculation after Ref. 48) and parity conservation. Nevertheless, it is not quite negligible for the bound states (states with strong interactions).

Without impurities, the  $e+h$  and  $2e+h$  eigenstates of  $H$  are labeled by total angular momentum  $L$  and its projection  $L_z$ . When converting these quantities to the planar geometry, neutral and charged states must be treated differently:  $L$  of an  $e-h$  pair represents the wave vector  $q=L/R$ , and for a  $2e+h$  state it corresponds to  $M=L-Q$ . The  $2e+h$  eigenstates are also labeled by spin  $S$  of the pair of electrons and its projection  $S_z$ . The calculation need only be performed in the  $L_z=S_z=0$  subspace, and the appropriate Zeeman shift can be added at the end to the energies of each triplet ( $S=1$ ) state.

With an impurity placed at a north pole of the sphere,  $L_z$  is still conserved, but  $L$  is not. Only the  $S_z=0$  subspace need be considered, but a separate diagonalization must be performed for each  $L_z$ .

The  $2e+h$  diagonalization was carried out in configuration-interaction basis,  $|i, j; k\rangle = c_i^\dagger c_j^\dagger c_k^\dagger |\text{vac}\rangle$ . Here indices  $i$  and  $j$  denote the occupied electron states,  $k$  describes the hole, and  $|\text{vac}\rangle$  is the vacuum state. Similarly, the basis for the  $e+h$  calculation was  $|i; k\rangle$ . As mentioned earlier, only the spin-unpolarized states with  $L_z \equiv m_i + m_j - m_k = 0$  are included in the basis. To find eigenstates corresponding to given  $(L, S)$  we used a modified Lanczos algorithm, with additional projection of Lanczos vectors at each iteration.

### III. RESULTS AND DISCUSSION

#### A. Density of states

We begin by the calculation of the density of states  $\text{DOS} = d\Gamma/dE$  (the number of states  $\Gamma$  per unit of energy  $E$ ). In Fig. 1 we compare the results for  $e+h$  and  $2e+h$  obtained for a rather large  $2Q=50$  and including only the lowest two

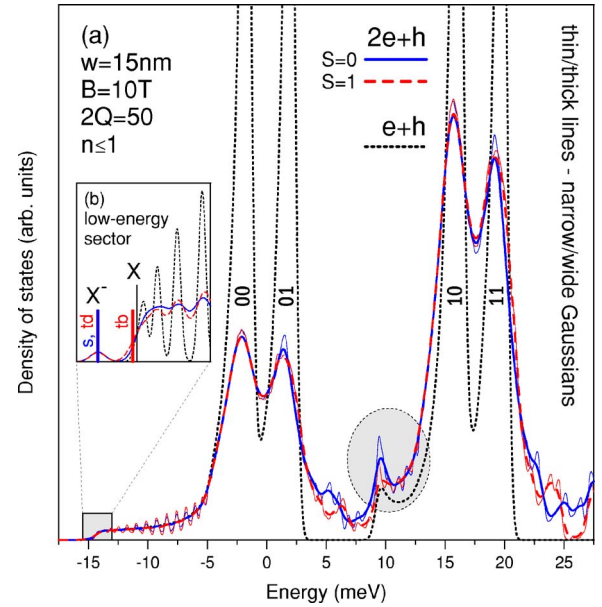


FIG. 1. (Color online) Density of states of  $e+h$  and  $2e+h$  systems in a symmetric GaAs quantum well of width  $w=15$  nm at magnetic field  $B=10$  T, calculated on a Haldane sphere with a large magnetic monopole strength  $2Q=50$  including only the two lowest electron and hole LL's ( $n \leq 1$ ). Solid curves were obtained from finite-size discrete energy spectra by Gaussian broadening. For  $2e+h$ , the DOS is divided by  $g=2Q+1$  (LL degeneracy of the second electron), and singlet and triplet configurations (spin  $S=0$  and 1) are drawn separately. For  $e+h$ , LL indices “ $n_e n_h$ ” mark the strongest peaks. Inset: magnified lowest-energy sector (vertical lines mark position of discrete bound triions and the excitonic ground state).

electron and hole LL's ( $n \leq 1$ ). The discrete energy spectra obtained from finite-size calculation were converted to the solid lines shown in the figure by broadening with Gaussians,

$$\text{DOS}(E) = \sum_i \mathcal{G}_\delta(E - E_i), \quad (2)$$

where the summation goes over all energy levels  $E_i$  and  $\mathcal{G}_\delta(x) = \delta^{-1} \pi^{-1/2} \exp(-x^2/\delta^2)$ . Thin and thick lines correspond to two different broadening widths  $\delta=0.2$  and  $0.5$  meV. Blue solid, red dashed, and black dotted lines were used to distinguish  $2e+h$  ( $S=0$  and 1 plotted separately; only  $S_z=0$  is shown for  $S=1$ ) from  $e+h$ . To compare the DOS for  $e+h$  and  $2e+h$ , the latter curve was rescaled from the value defined by Eq. (2) by  $g^{-1}=(2Q+1)^{-1}$  (i.e., divided by the number of states available to the second electron). Energy  $E$  is measured from the noninteracting configurations in the lowest LL.

For a noninteracting  $e-h$  pair, the DOS consists of discrete peaks labeled by the LL indices for both particles, “ $n_e n_h$ .” The black dotted curve demonstrates the effect of the  $e-h$  interaction. Within each pair of LL's, magnetoexcitonic dispersion becomes flat at long wave vectors  $q$ , corresponding to the vanishing  $e-h$  attraction. Therefore, although smeared toward lower energies, strong “ $n_e n_h$ ” peaks persist. In our calculation, the restricted area of the sphere prohibits the pair

to separate in the  $q \rightarrow \infty$  limit (the range of  $q=L/R$  is restricted by  $L \leq 2Q$ ) and the “ $n_e n_h$ ” peaks have finite height and are displaced to the left by the remnant attraction ( $\sim e^2/2R = (2\sqrt{Q})^{-1} e^2/\lambda$ ). This redshift ( $\sim 1.4$  meV for  $2Q=50$ ) is a finite-size artifact. The low-energy tail extends from each “ $n_e n_h$ ” peak over the range of the excitonic binding energy within the corresponding pair of LL’s. Since  $e^2/\lambda$  is larger than  $\hbar\omega_c$  of the holes, these tails essentially close the gaps between the neighboring hole LL’s. Thin lines (shown in the magnified low-energy sector in the inset) reveal artificial size quantization on a sphere ( $L=0, 1, 2, \dots$ ). On the other hand, an interesting *real* feature is the maximum at the beginning of the “10” tail ( $E \approx 10$  meV). It is due to the fact that excitonic dispersion for  $n_e \neq n_h$  is nonmonotonic at small wave vectors  $q$  (the ground state occurs at  $q > 0$ , leading to  $dE/dq=0$  and  $d\Gamma/dq \propto q > 0$ —i.e., to a singularity in  $d\Gamma/dE$ ).

The curves for  $2e+h$  are also dominated by the noninteracting peaks “ $n_e n_h$ ” corresponding to three unbound particles confined to different combinations of LL’s. Low-energy tails describe the exciton with an additional unbound electron (note oscillations due to excitonic size quantization). Bound trion states appear as discrete peaks below the continuous tails, well visible only in the inset, additionally marked with red and blue bars. All three trions  $X_s^-$ ,  $X_{td}^-$ , and  $X_{tb}^-$  appear bound (the excitonic ground state is marked by a black bar for comparison). However, weak ( $< 1$  meV) binding of  $X_s^-$ , virtually equal to  $X_{td}^-$ , is an artifact of the unrealistic  $n \leq 1$  restriction.

The emergence of bound trion states below the exciton’s continuum is one noticeable difference between the  $e+h$  and  $2e+h$  DOS. Another significant effect of the exciton-electron interaction is further (compared to one due to excitonic  $e-h$  interaction) smearing of the LL’s—i.e., transfer of the density of states away from LL’s and filling the gaps between them. Also, the DOS within the inter-LL regions shows features related to the interactions in a nontrivial manner. For example, the spin dependence of structures at  $E \approx 5$  meV and  $E \approx 25$  meV reveals their connection with the (obviously spin-sensitive) exciton-electron interaction. Note that the  $e+h$  peak at  $E \approx 10$  meV, identified earlier with an inter-LL exciton, persists in the  $2e+h$  curves regardless of spin configuration (to confirm its *one*-electron nature).

The  $n \leq 1$  restriction to only two lowest LL’s was helpful in demonstrating LL smearing and the emergence of additional peaks between LL’s due to the  $e-h$  and  $X-e$  interactions used in Figs. 1 and 2. However, it gives incorrect exciton and trion energies and, more importantly, ignores the contribution to the DOS coming from the neglected higher hole LL’s (recall that the hole’s  $\hbar\omega_c$  is only 3.7 meV at  $B=10$  T, much smaller than the electron’s, 17.8 meV).

More accurate trion binding energies (for both  $X^-$  and  $X^+$ ) are plotted in Fig. 2 as a function of  $B$ . These values were obtained by including five LL’s ( $n \leq 4$ ) and up to two subbands ( $s \leq 1$ ) for each electron and hole. The lowest-subband ( $s=0$ ) calculation is similar to Ref. 30, but it used more accurate Coulomb matrix elements, calculated for the actual  $\chi_0(z)$ . For  $X^-$ , an additional weakly bound “dark singlet” state occurs only at quite high fields. The curves for  $s \leq 1$

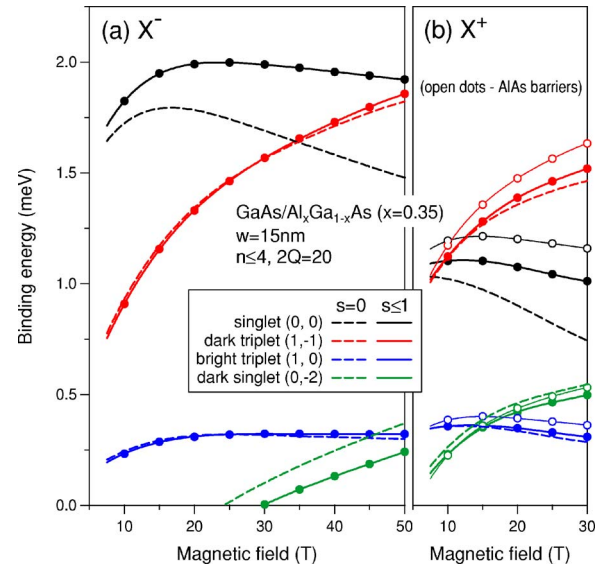


FIG. 2. (Color online) Binding energies  $\Delta$  of four different negative (a) and positive (b) trions  $X^\pm$  (the pair of labels in parentheses are the two-electron spin  $S$  and total angular momentum  $M$ ) in a symmetric GaAs quantum well of width  $w=15$  nm as a function of magnetic field  $B$ , calculated on a Haldane sphere with a magnetic monopole strength  $2Q=20$  including five lowest LL’s ( $n \leq 4$ ) and either one ( $s=0$ ) or two lowest subbands ( $s \leq 1$ ) for each electron and hole. Solid curves were obtained by interpolation from exact diagonalization at the values of  $B$  marked with dots.

demonstrate that in a narrow symmetric well subband mixing is most efficient for the  $M=0$  singlet, while the lowest-subband approximation is accurate for both triplets.

In our calculations we assumed an Al fraction of  $x=0.35$  in the  $\text{Al}_x\text{Ga}_{1-x}\text{As}$  barriers. This restriction is justified by the fact that the binding energies of  $X^-$  are almost insensitive to the increase of the Al fraction all the way up to  $x=1$ . The only exception is data for  $X^+$  marked with open dots in Fig. 2(b), obtained for pure AlAs barriers. Evidently, the  $X^+$  binding energies depend more strongly on the barrier height, which must be taken into account in a realistic model.

A more accurate DOS is shown in Fig. 3, including five LL’s ( $n \leq 4$ ), but still only the lowest subband. Since the dimension of the Hilbert space quickly grows with  $n_{\text{max}}$  and  $2Q$ , we were forced to use a smaller  $2Q=20$  in this case (for  $2e+h$  this yields a dimension of 58 875 for the  $L_z=S_z=0$  subspace, *all* of whose eigenenergies must be calculated to plot the DOS). Especially at higher energies, the curves would become very complicated due to an increasing number of overlapping peaks corresponding to different combinations of  $n_e$  and  $n_h$ —if not only 5, but *all* LL’s were included for the hole. By counting electron cyclotron gaps from the lowest LL peak at  $E \approx -e^2/2R$ , energies corresponding to consecutive  $n_e$ ’s have been marked with gray vertical lines. Comparison of the curves for  $e+h$  (here plotted without rescaling by  $g^{-1}$ ) and  $2e+h$  shows that the effect of smearing the LL’s and filling the gaps between them due to the  $X-e$  interaction is only enhanced when more LL’s are included. In the inset, the binding energies of all trion peaks are already well converged for  $n \leq 4$  (note, however, that the lowest-subband approximation considerably affects espe-

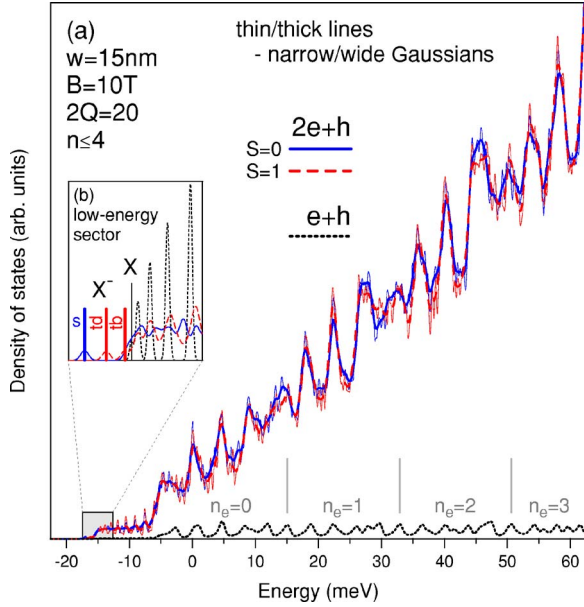


FIG. 3. (Color online) The same as in Fig. 1 but for  $2Q=20$ ,  $n_s \leq 4$ , and without dividing the  $2e+h$  DOS by  $g=2Q+1$ .

cially the singlet state); the exact values are  $\Delta=1.72$ ,  $0.93$ , and  $0.24$  meV for  $X_s^-$ ,  $X_{id}^-$ , and  $X_{ib}^-$ , respectively.

An ionized impurity can have a similar effect on the  $e+h$  DOS to that of an additional electron. This impurity can be either a positive or negative point charge (ionized donor  $D^+$  or ionized acceptor  $A^-$ ) placed at a distance  $d$  away from the center of the quantum well. The effects of  $D^+$  and  $A^-$  are not equivalent due to the  $e-h$  asymmetry. Two frames of Fig. 4 show how the  $e+h$  DOS changes in the presence of  $D^+$  or  $A^-$  placed at  $d/w=1/2$  and  $0$  (edge and center of the well). In the plotted energy range (up to the first excitonic maximum “00”), the curves for  $d/w=1$  are almost identical to those without an impurity. One or more bound  $D^+X$  or  $A^-X$  states (analogous to trions) emerge below the excitonic tail, at the position sensitive to  $d$ . Being localized (and nondegenerate), they do not contribute to the macroscopic DOS.

When the impurity approaches the well, a strong peak detaches from “00” and moves to the left through the excitonic tail. It corresponds to the (macroscopically degenerate)  $D^0+h$  or  $A^0+e$  configuration with the unbound  $e-h$  pair. In our example, it passes the tail’s edge ( $X$  ground state) when the impurity is already inside the well, at  $d \approx 3$  nm for  $D^+$  and  $5.5$  nm for  $A^-$ . For  $d=0$ , especially the  $A^0$  is bound much more strongly than  $X$ . Thus, the strongest effect of an impurity is that, depending on  $d$ , it can bring down the macroscopic DOS corresponding to the unbound  $e-h$  below the free excitonic ground state. Certainly, the localized  $D^+X$  and  $A^-X$  states involving the  $e-h$  binding still remain the absolute ground states. Here, the qualitative difference caused by the impurity is that the DOS rises abruptly from essentially zero at the nondegenerate bound state to the continuum of degenerate unbound states (instead of through an excitonic tail). Especially the marginally bound  $A^-X$  is hardly distinguished from the continuum.

For  $d=0$  we have also marked the  $D^0+h^*$  and  $A^0+e^*$  peaks corresponding to the unbound hole or electron in a

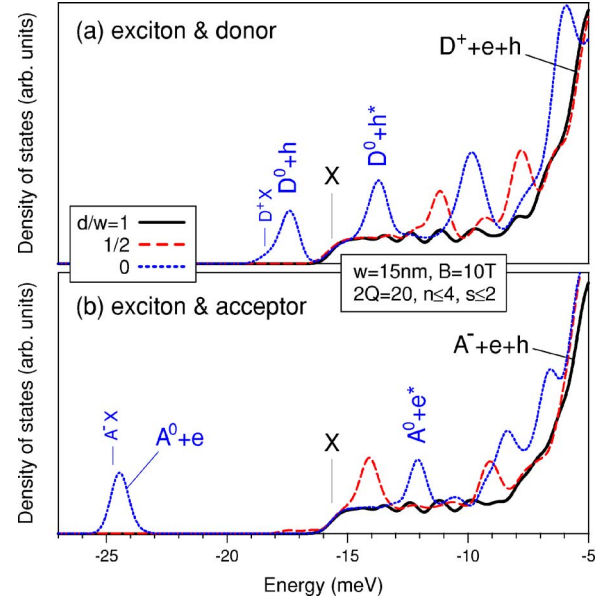


FIG. 4. (Color online) Density of states of  $e+h$  in a symmetric GaAs quantum well of width  $w=15$  nm at magnetic field  $B=10$  T in the presence of a positive (a) and negative (b) impurity at different distances  $d$  from the center of the well, calculated on Haldane sphere with magnetic monopole strength  $2Q=20$  including five LL’s ( $n_s \leq 4$ ) and three subbands ( $s \leq 2$ ) for electrons and holes. Solid curves were obtained by Gaussian broadening. Marked bound states:  $D^0=D^++e$ ,  $D^+X=D^++X$ ,  $A^0=A^-+h$ , and  $A^-X=A^-+X$ ;  $e^*$  and  $h^*$  denote electron and hole in the excited ( $n=1$ ) LL.

higher LL and thus originating from the “01” and “10” peaks without an impurity. These peaks are separated from  $D^0+h$  and  $A^0+e$  by a cyclotron gap; thus, an impurity mixes the LL peak structure with an excitonic tail due to  $e-h$  interaction.

## B. Oscillator strength

Let us now turn to the calculation of oscillator strength  $\Omega$  for the  $\text{vac} \leftrightarrow e+h$  and  $e \leftrightarrow 2e+h$  optical transitions (“ $\rightarrow$ ” for absorption, “ $\leftarrow$ ” for emission). For a pair of initial and final states—e.g.,  $\psi=e$  and  $\phi=2e+h$ —it is calculated from Fermi’s golden rule,

$$\Omega_{\psi\phi} = \sum_k |\langle \phi | c_k^\dagger c_{\bar{k}}^\dagger | \psi \rangle|^2. \quad (3)$$

Here,  $k=[\beta, n, m, \sigma]$  and  $\bar{k}=[\bar{\beta}, n, -m, -\sigma]$ , and the summation runs over all electron states  $k$  in the conduction band and all corresponding hole states  $\bar{k}$  in the valence band. Note that according to convention of Eq. (1),  $c_k^\dagger$  creates electrons or holes, depending on the band index  $\beta$ , leading to the reversed sign of  $m$  and  $\sigma$  in  $\bar{k}$ . The oscillator strength for the recombination of initial  $\phi=e+h$  or  $2e+h$  states, in the latter case summed over all final  $\psi=e$  states, can be expressed as a function of the initial energy  $E=E_\phi$ ,

$$\Omega(E) = \sum_{\psi\phi} \Omega_{\psi\phi} \delta(E_\phi - E). \quad (4)$$

This is the  $e+h$  or  $2e+h$  “optical density of states” (ODOS). Alternatively, oscillator strength (if necessary, weighted by

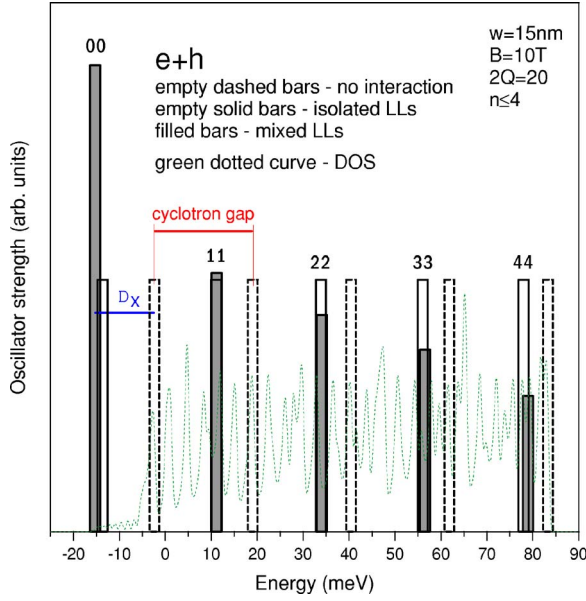


FIG. 5. (Color online) Optical density of states of  $e+h$ , equivalent to absorption spectrum of an exciton, in a symmetric GaAs quantum well of width  $w=15$  nm at magnetic field  $B=10$  T, calculated on a Haldane sphere with a magnetic monopole strength  $2Q=20$  including the five lowest electron and hole LL's ( $n \leq 4$ ). Results without an  $e-h$  interaction, with an interaction within isolated LL's (peaks marked with LL indices " $n_e n_h$ "), and with all interaction effects (including both intra- and inter-LL scattering) are shown. The  $e+h$  DOS from Fig. 3 is drawn for reference.

the occupation function  $\Theta_\psi$  for the initial states  $\psi=e$  can be expressed as a function of the photon energy  $\mathcal{E}=E_\phi-E_\psi$ ,

$$\Omega(\mathcal{E}) = \sum_{\psi\phi} \Omega_{\psi\phi} \Theta_\psi \delta(E_\phi - E_\psi - \mathcal{E}). \quad (5)$$

This is the  $\psi \rightarrow \phi$  absorption spectrum (equivalent to  $\phi$ 's ODOS for  $\psi=vac$ , but not for  $\psi=e$ ).

In Fig. 5 we plot the ODOS of  $e+h$ . The parameters ( $w=15$  nm and  $B=10$  T) and Hilbert space ( $n \leq 4$  and  $2Q=20$ ) are the same as in Fig. 3. If the Coulomb energy  $e^2/\lambda$  were much smaller than the cyclotron gaps, then the only optically active states would be the  $q=0$  excitons with electrons and holes confined to the same LL's ( $n_e=n_h \equiv n$ ). As shown with empty bars, these excitonic peaks " $nn$ " in  $\Omega(\mathcal{E})$  would have equal height and occur at  $E(n)=n\hbar(\omega_{c,e}+\omega_{c,h})-\Delta_X(n)$ , where  $\Delta_X(n)$  is the exciton binding energy in the  $n$ th LL. These energies coincide with the low-energy edges of the excitonic tails of the " $nn$ " peaks in DOS (replotted with a thin dotted line), where degeneracy is absent and the DOS vanishes. Since the exciton binding  $\Delta_X(n)$  decreases as a function of  $n$ , the separation between consecutive peaks also decreases and it is always larger than the cyclotron gap between the corresponding " $nn$ " maxima in the DOS. For  $w=15$  and  $B=10$  T, the distances between peaks "00," "11," and "22" (calculated excluding LL mixing by setting  $v_{ijkl}=0$  unless  $n_i=n_j=n_k=n_l \equiv n$ ) are  $E_{11}-E_{00}=24.7$  meV and  $E_{22}-E_{11}=22.8$  meV, both considerably larger than  $\hbar(\omega_{c,e}+\omega_{c,h})=21.5$  meV.

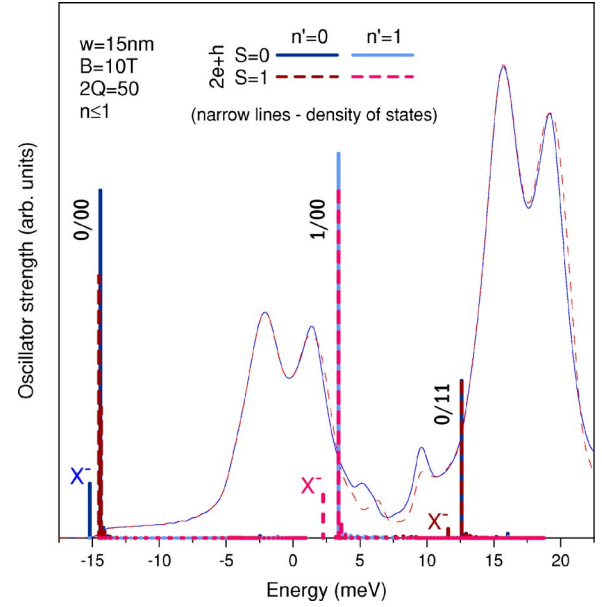


FIG. 6. (Color online) Optical density of states of  $2e+h$ , in a symmetric GaAs quantum well of width  $w=15$  nm at magnetic field  $B=10$  T, calculated on a Haldane sphere with a large magnetic monopole strength  $2Q=50$  including only the two lowest electron and hole LL's ( $n \leq 1$ ). Singlet and triplet initial  $2e+h$  spin configurations ( $S=0$  and  $1$ ) and ground and excited final  $e$  states ( $n'=0$  and  $1$ ) are drawn with different lines. Strongest peaks are marked by LL indices of the initial and final states, " $n'/n_e n_h$ " with  $n_e=n_h$ . Weak peaks associated with bound trions ( $X^-$ ) are also indicated. The  $2e+h$  DOS from Fig. 1 is drawn for reference.

In reality, inter-LL scattering mixes  $q=0$  states with different  $n$ . As shown with solid bars, this causes a shifting of the peaks (and a further small increase of the spacing between neighboring peaks) and transfer of oscillator strength from higher to lower energy. Nevertheless, the effect is perturbative and consecutive peaks can still be labeled by  $n$ . For  $w=15$  and  $B=10$  T, the first two gaps in  $\Omega$  (calculated including all matrix elements  $v_{ijkl}$ ) increase to  $E_{11}-E_{00}=26.4$  meV and  $E_{22}-E_{11}=23.0$  meV. The relative magnitudes of the lowest three peaks are  $\Omega_{11}/\Omega_{00}=0.55$  and  $\Omega_{22}/\Omega_{00}=0.46$ .

In Fig. 6 we plot the ODOS of  $2e+h$  calculated using the same Hilbert space ( $n \leq 1$  and  $2Q=50$ ) as in Fig. 1. Also for this larger system there is no apparent correlation between the features in the DOS and ODOS. This follows immediately from the  $q=0$  selection rule, equivalent to the requirement of nondegenerate relative motion of the recombining  $e-h$  pair, preventing a high DOS of a  $2e+h$  state involving such a pair.

In analogy to  $e+h$ , the main peaks can be labeled by " $n'/nn$ ," and they correspond to a  $q=0$  exciton created or annihilated on the  $n$ th LL, in the presence of the second,  $\psi$  electron on the  $n'$ th LL. In those main peaks " $n'/nn$ ," the second electron is not bound to the created or annihilated exciton; they describe excitonic optical processes, weakly affected by the exciton-electron scattering. Optically active bound trions (with electrons and holes in different LL's) appear in the form of weaker peaks displaced from " $n'/nn$ " by

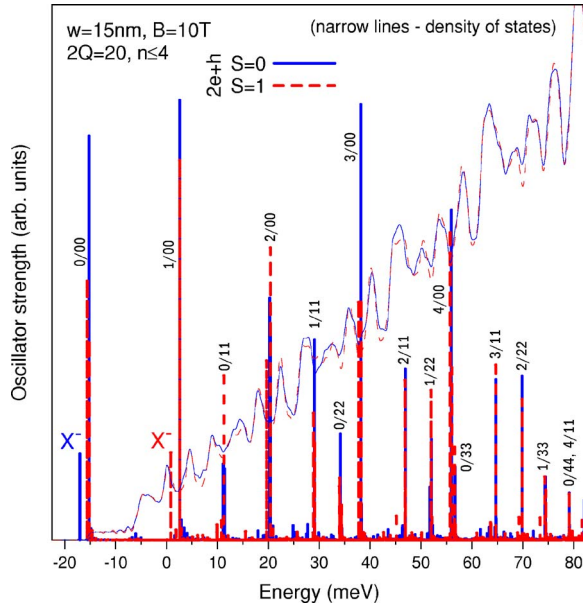


FIG. 7. (Color online) The same as in Fig. 6 but for  $2Q=20$  and  $n \leq 4$ . The strongest peaks are identified as excitonic “ $n'/nn$ ” transitions or trion recombination ( $X^-$ ).

the binding energy. In the lowest LL, the only well-resolved trion is the singlet (dark triplet by definition has  $\Omega=0$  and bright triplet is too weakly bound to be distinguished from exciton in this energy scale). In the triplet trion at  $E \approx 2.5$  meV one of the electrons is in the  $n=1$  LL. Although unstable against inter-LL relaxation, this state can form by capturing a “00” photoexciton by a thermally excited electron.

Note that “shake-up” transitions<sup>49</sup> ( $n'/nn \leftrightarrow n''$  with  $n' \neq n''$ )—i.e., a combination of “ $nn$ ” recombination with  $n' \leftrightarrow n''$  cyclotron excitation of the second electron) are forbidden<sup>50</sup> for an isolated trion due to invariance under 2D (magnetic) translations. This selection rule does not preclude replicas of an exciton and an *unbound* second electron, but these transitions have negligible intensity for  $\nu \sim g^{-1} \ll 1$  and cannot be identified in Fig. 6.

Figure 7 is similar to Fig. 6, but it shows the  $2e+h$  ODOS calculated with five LL's taken into account ( $n \leq 4$  and  $2Q=20$ ). The picture becomes fairly complicated, but the idea is the same. Dominant peaks correspond to excitonic transitions and can be labeled by “ $n'/nn$ ” (in the calculated spectrum, the assignment is straightforward due to angular momentum conservation in the optical transition, here causing the  $L=Q+n'$  selection rule). A great number of weaker transitions that involve an exciton-electron interaction emerge around the excitonic peaks. In particular, bright trions appear below “0/00” and “1/00” (singlet and triplet, respectively).

Figure 8 presents the  $2e+h$  absorption spectra  $\Omega(\mathcal{E})$ , calculated assuming that an electron in the initial state is either in the lowest LL (ground state) or in a higher  $n=1$  LL (due to thermal excitation). To observe the superposition of many closely spaced small peaks, each discrete  $e \rightarrow 2e+h$  transition was broadened with a Gaussian of width  $\delta=0.5$  meV (main frames) or 0.2 meV (insets). As a reference, the  $\text{vac} \rightarrow e+h$  excitonic spectrum is shown with gray bars.

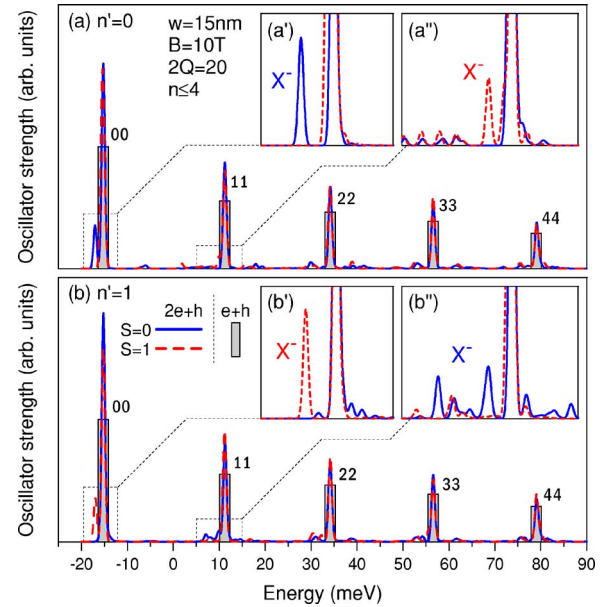


FIG. 8. (Color online)  $2e+h$  absorption spectra in a symmetric GaAs quantum well of width  $w=15$  nm at magnetic field  $B=10$  T, calculated on a Haldane sphere with a magnetic monopole strength  $2Q=20$  including five lowest electron and hole LL's ( $n \leq 4$ ). Solid curves were obtained by Gaussian broadening. Singlet and triplet  $2e+h$  spin configurations ( $S=0$  and 1) are drawn separately. Frames (a) and (b) correspond to the initial-state electron in the lowest or first excited LL ( $n'=0$  or 1). The strongest peaks marked as “ $nn$ ” correspond to excitonic absorption in the  $n$ th LL ( $e+h$  absorption spectrum from Fig. 5 is shown with gray bars for reference). Insets show magnified regions around the lowest two peaks “00” and “11.” Trion peaks ( $X^-$ ) are identified.

The main result is that when the (great number of) main ODOS peaks “ $n'/nn$ ” are shifted by  $E_\psi = n' \hbar \omega_{c,e}$  to convert  $\Omega(E)$  into  $\Omega(\mathcal{E})$ , they all fall exactly onto the absorption spectrum of a bare exciton. The presence of an additional electron does not cause a shifting or splitting of these main absorption lines, and it has an insignificant effect on their relative intensities. This demonstrates that, somewhat surprisingly, bare excitonic absorption is unaffected by a dilute electron gas (neither by renormalization of energy nor by transfer of intensity between LL's). This result is obtained for a realistic quantum well, with significant electron-hole asymmetry and LL mixing.

The effect of free electrons is the emergence of additional (compared to the bare exciton) features in the absorption spectrum, the strongest of them associated with the formation of trions. In Fig. 8, trion absorption peaks can be seen most clearly in the insets, in which the vicinities of peaks “00” and “11” have been magnified. In reality, their intensity relative to the excitonic peaks will depend on the filling factor and can be much higher than in our model (which represents a very dilute system with only one free electron per  $g=2Q+1$  states of the lowest LL). Remarkably, the spin of the strong trion-related features correlates with the parity of  $n' - n$ : singlet ( $S=0$ ) peaks appear for  $n'=0$  below “00” and for  $n'=1$  below “11,” while triplets ( $S=1$ ) occur for the opposite combinations of  $n'=0$  with “11” and  $n'=1$  with “00.”

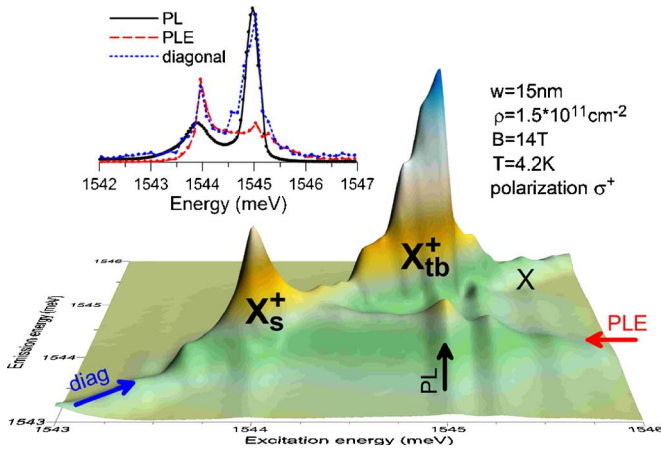


FIG. 9. (Color online) Polarized photoluminescence-excitation spectrum measured in a symmetric  $w=15$  nm GaAs quantum well with hole concentration  $\rho=1.5 \times 10^{11} \text{ cm}^{-2}$ , in magnetic field  $B=14$  T, at temperature  $T=4.2$  K.

#### IV. EXPERIMENT

To verify some of the presented calculations we performed polarization-resolved photoluminescence and photoluminescence-excitation experiments on a symmetric  $w=15$  nm GaAs/AlAs quantum well, containing a valence hole gas with concentration  $\rho=1.5 \times 10^{11} \text{ cm}^{-2}$  and subject to a strong magnetic field. The PLE experiment consisted of measuring polarization-resolved PL (emission intensity  $I$  as a function of emission energy  $\mathcal{E}_{\text{out}}$ ) for a series of excitation energies  $\mathcal{E}_{\text{in}}$ . The spectra presented in Fig. 9 were recorded at  $T=4.2$  K, in Faraday configuration, at  $B=14$  T ( $\nu \approx 0.45$ ), and for the circular  $\sigma^+$  polarization of light (corresponding to optical transitions of an electron in the excited spin state). The emission intensity  $I$  is plotted as a function of both  $\mathcal{E}_{\text{in}}$  and  $\mathcal{E}_{\text{out}}$ . In the inset we showed the following three cross sections. (i) The PL (emission) spectrum is  $I(\mathcal{E}_{\text{out}})$  for a fixed, high  $\mathcal{E}_{\text{in}}$ . Although it is typically measured for a much higher  $\mathcal{E}_{\text{in}}$ , here we plot the data corresponding to resonant excitation of  $X_{\text{tb}}^+$ . (ii) The PLE spectrum is  $I(\mathcal{E}_{\text{in}})$  for a fixed, low  $\mathcal{E}_{\text{out}}$ , here corresponding to the  $X_s^+$  recombination. For a regular dependence of the relaxation on  $\mathcal{E}_{\text{in}}$ , PLE is an indirect measure of absorption. (iii) The diagonal cross section  $I(\mathcal{E}_{\text{out}}=\mathcal{E}_{\text{in}})$ , usually difficult to detect due to the strong reflection of the incident light from the surface. By smoothing and appropriate orientation of the surface with respect to the incident and reflected directions we were able to minimize this effect and record meaningful diagonal spectra.

In Fig. 9, two strong peaks correspond to two optically active trions,  $X_s^+$  and  $X_{\text{tb}}^+$ . Other minor features are artifacts (note a sizable 0.12-meV step in  $\mathcal{E}_{\text{in}}$ ). The suppressed intensity of the  $X$  (whose position relative to the  $X^+$ s is anticipated from the following Fig. 10) relative to the bright  $X^+$ s results from a rather large hole concentration. On the other hand, the strongest  $X_{\text{tb}}^+$  peak along the diagonal confirms an earlier theoretical prediction for the trion oscillator strengths.<sup>30</sup>

In Fig. 10, we plot a pair of polarized  $\sigma^-$  and  $\sigma^+$  PL spectra  $I(\mathcal{E}_{\text{out}})$ . They were recorded in the same sample and

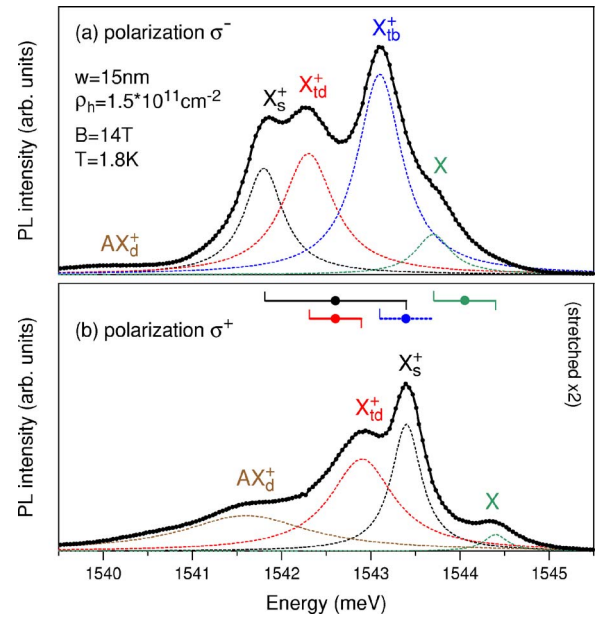


FIG. 10. (Color online) Polarized photoluminescence spectra measured in a symmetric  $w=15$  nm GaAs quantum well with hole concentration  $\rho=1.5 \times 10^{11} \text{ cm}^{-2}$ , in magnetic field  $B=14$  T, at temperature  $T=1.8$  K.

at the same magnetic field as PLE of Fig. 9, but for a higher excitation energy  $\mathcal{E}_{\text{in}}=2.57$  eV (wavelength 488 nm) and at low temperature  $T=1.8$  K. Three trion states ( $X_s^+$ ,  $X_{\text{td}}^+$ , and  $X_{\text{tb}}^+$ ) along with the exciton are identified for the  $\sigma^-$  polarization. In the  $\sigma^+$  spectrum, the  $X_{\text{td}}^+$  peak is weakened and  $X_{\text{tb}}^+$  disappears completely due to spin polarization. Additional low-energy peaks marked as  $AX_d^+=A^0+X^+$  show the recombination of a spin doublet ( $S=\frac{1}{2}$ ) ground state of a trion bound to a neutral acceptor located inside the well (cf. Fig. 4); such impurity-bound trions are discussed elsewhere.<sup>51</sup>

The unambiguous assignment of the peaks was possible from the analysis of the field evolution of the spectra, from  $B=0$  beyond  $B=14$  T, presented in a separate publication.<sup>51</sup> As noted by Glasberg *et al.*,<sup>15</sup> the Zeeman splitting of different  $X$  and  $X^+$  states is very different (because of the wave vector dependence of the Landé  $g$  factor for the holes). We marked these splittings with color horizontal bars in Fig. 10(b). The large value of 1.6 meV for  $X_s^+$  (and  $AX_d^+$ ) compared to only 0.7 meV for  $X$  and 0.6 meV for  $X_{\text{td}}^+$  is related to the occupation of a strongly repulsive zero-angular-momentum hole pair state, characteristic of the singlet trion (and of doublet  $AX^+$ ). The analysis of the pair-correlation function shows that this pair state is not occupied also in  $X_{\text{tb}}^+$  (despite the triplet spin configuration). This leads us to expect similar  $X_{\text{tb}}^+$  and  $X_{\text{td}}^+$  Zeeman splittings, even though  $X_{\text{tb}}^+$  is only detected in one polarization.

Knowing the difference between  $X$  and  $X^+$  Zeeman splittings is necessary for a meaningful comparison of the trion binding energies  $\Delta$  with the calculation of Fig. 2(b) in which the Zeeman energy was ignored. The Coulomb binding energies  $\Delta$  are extracted from the experimental PL spectra by comparing the average  $X$  and  $X^+$  energies measured in both polarizations,<sup>15</sup> in Fig. 10(b) marked by dots on the Zeeman bars. In this way, we find  $\Delta_s^+=\Delta_{\text{td}}^+ \approx 1.4$  meV and  $\Delta_{\text{tb}}^+$



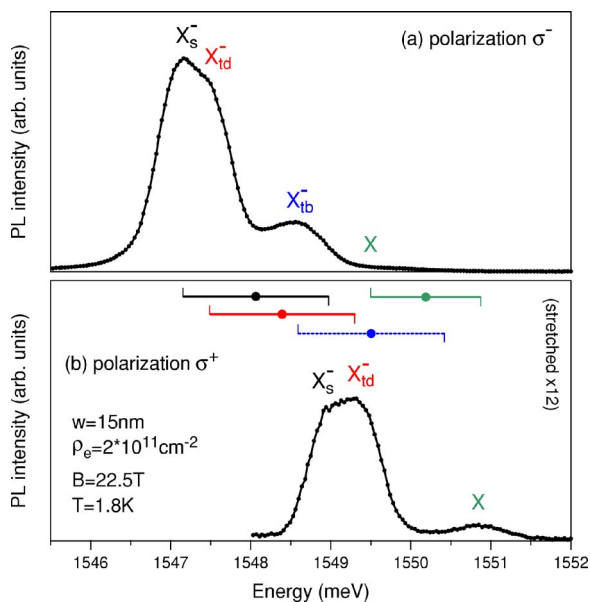


FIG. 11. (Color online) Polarized photoluminescence spectra measured in a symmetric  $w=15$  nm GaAs quantum well with electron concentration  $\rho=2 \times 10^{11} \text{ cm}^{-2}$ , in magnetic field  $B=22.5$  T, at temperature  $T=1.8$  K.

$\approx 0.6$  meV. Compared to these values, the  $x=1$  calculation of Fig. 2(b) predicting  $\Delta=1.2$ , 1.35, and 0.4 meV, respectively, slightly underestimates the binding of all three states. The slight discrepancy could result from including only two lowest quantum well subbands and five lowest LL's, assuming equidistant LL's also for the holes and ignoring the light-hole and heavy-hole mixing, all likely to enhance binding. Numerical tests indicate that neither higher subbands ( $s \geq 2$ ) nor the variation of LL spacing (beyond  $n=1$ ) play a role, but the  $n \leq 4$  restriction indeed has a noticeable ( $\leq 0.2$  meV) effect on  $\Delta$ .

The spectra in Fig. 11 are analogous to Fig. 10, but they were recorded on an electron gas and involve negative trions. The sample is also a symmetric  $w=15$  nm GaAs quantum well, but the concentration is slightly higher,  $\rho=2 \times 10^{11} \text{ cm}^{-2}$ , so we had to use a stronger field,  $B=22.5$  T, to keep a sufficiently low filling factor,  $\nu \approx 0.4$ . In both polarizations, the detected trions correspond to those of Fig. 10. The weak  $X$  peak marked for  $\sigma^-$  can be identified more convincingly when the intensity is plotted in a logarithmic scale. The Zeeman splittings found in this system are 1.8 meV for  $X_s^-$  and  $X_{id}^-$  (the same value was hence assumed for  $X_{tb}^-$ ) and 1.4 meV for  $X$ . Weaker variation of the splitting supports its attribution to the occupation of two-hole states. Using these splittings, we find the following Coulomb trion binding en-

ergies:  $\Delta_s^- \approx 2.1$  meV,  $\Delta_{td}^- \approx 1.8$  meV, and  $\Delta_{tb}^- \approx 0.65$  meV. Again, the calculation of Fig. 2(a) predicting  $\Delta=2$ , 1.4, and 0.3 meV, respectively, slightly underestimates all these values.

## V. CONCLUSION

We have carried out exact numerical diagonalization of realistic  $e+h$  and  $2e+h$  Hamiltonians (including spin, Coulomb interactions, and mixing of LL's and quantum well subbands) on a Haldane sphere. The parameters used for illustration are adequate for a symmetric 15-nm GaAs quantum well in a magnetic field  $B=10$  T.

The calculation of trion binding energies has been considerably advanced by taking the actual subband wave functions for the integration of Coulomb matrix elements and by including five LL's and two quantum well subbands for each electron and hole in the exact diagonalization.

From the full energy spectra we have calculated the density of states. The main difference between the DOS of  $e+h$  and  $2e+h$ , representative of excitons with and without the presence of additional free electrons, is the emergence of discrete bound trion states below the excitonic tails and redistribution of the DOS away from the LL peaks and filling the gaps between them. The effect of an impurity on the  $e+h$  DOS is also studied as a function of its charge and position in the well.

For the full spectra of eigenstates, we have calculated the optical oscillator strength  $\Omega$ . The optical density of states of  $2e+h$  shows no obvious correlation with the DOS. It is fairly complicated, with a great number of strong transitions labeled by LL indices of the recombining  $e-h$  pair and of the leftover electron. However, the  $e \rightarrow 2e+h$  absorption spectrum is far simpler. It is dominated by a series of LL peaks for the purely excitonic transitions  $vac \rightarrow e+h$ . These main peaks are neither shifted in energy nor is their intensity noticeably suppressed or enhanced. The presence of (and interaction with) an additional electron shows in the form of additional weaker peaks. Some of them are attributed to bound trion states (in the lowest and higher LL's).

The numerical results have been successfully compared with PL and PLE experiments carried out on 2D hole and electron gases. In particular, the absorption and emission of the whole family of both negative and positive trions in the lowest LL has been observed.

## ACKNOWLEDGMENTS

A.W. thanks J. J. Quinn for helpful discussions. This work was supported by Grant Nos. 1P03B03230 and N20210431/0771 (Polish MNiSW) and RITA-CT-2003-505474 (EC).

<sup>1</sup>M. A. Lampert, Phys. Rev. Lett. **1**, 450 (1958).

<sup>2</sup>K. Kheng, R. T. Cox, Y. Merle d'Aubigne, F. Bassani, K. Saminadayar, and S. Tatarenko, Phys. Rev. Lett. **71**, 1752 (1993).

<sup>3</sup>F. Bassani and G. P. Parravicini, *Electronic States and Optical*

*Transitions in Solids* (Pergamon, New York, 1975); E. L. Ivchenko, *Optical Spectroscopy of Semiconductor Nanostructures* (Alpha Science International Ltd., Oxford, 2005); P. Hawrylak and M. Potemski, Phys. Rev. B **56**, 12386 (1997).

- <sup>4</sup>G. A. Narvaez, P. Hawrylak, and J. A. Brum, *Physica E (Amsterdam)* **9**, 716 (2001).
- <sup>5</sup>S. Huant, S. P. Najda, and B. Etienne, *Phys. Rev. Lett.* **65**, 1486 (1990).
- <sup>6</sup>A. B. Dzyubenko, *Phys. Rev. B* **65**, 035318 (2002).
- <sup>7</sup>B. Stebe and A. Ainane, *Superlattices Microstruct.* **5**, 545 (1989).
- <sup>8</sup>H. Buhmann, L. Mansouri, J. Wang, P. H. Beton, N. Mori, L. Eaves, M. Henini, and M. Potemski, *Phys. Rev. B* **51**, 7969 (1995).
- <sup>9</sup>G. Finkelstein, H. Shtrikman, and I. Bar-Joseph, *Phys. Rev. Lett.* **74**, 976 (1995); *Phys. Rev. B* **53**, R1709 (1996).
- <sup>10</sup>A. J. Shields, M. Pepper, M. Y. Simmons, and D. A. Ritchie, *Phys. Rev. B* **52**, 7841 (1995).
- <sup>11</sup>D. Gekhtman, E. Cohen, A. Ron, and L. N. Pfeiffer, *Phys. Rev. B* **54**, 10320 (1996).
- <sup>12</sup>G. V. Astakhov, D. R. Yakovlev, V. P. Kochereshko, W. Ossau, J. Nürnberger, W. Faschinger, and G. Landwehr, *Phys. Rev. B* **60**, R8485 (1999); G. V. Astakhov, D. R. Yakovlev, V. P. Kochereshko, W. Ossau, W. Faschinger, J. Puls, F. Henneberger, S. A. Crooker, Q. McCulloch, D. Wolverson, N. A. Gippius, and A. Waag, *ibid.* **65**, 165335 (2002).
- <sup>13</sup>O. Homburg, K. Sebald, P. Michler, J. Gutowski, H. Wensch, and D. Hommel, *Phys. Rev. B* **62**, 7413 (2000).
- <sup>14</sup>A. J. Shields, J. L. Osborne, M. Y. Simmons, M. Pepper, and D. A. Ritchie, *Phys. Rev. B* **52**, R5523 (1995).
- <sup>15</sup>S. Glasberg, G. Finkelstein, H. Shtrikman, and I. Bar-Joseph, *Phys. Rev. B* **59**, R10425 (1999).
- <sup>16</sup>L. P. Gor'kov and I. E. Dzyaloshinskii, *Zh. Eksp. Teor. Fiz.* **53**, 717 (1967) [*Sov. Phys. JETP* **26**, 449 (1968)].
- <sup>17</sup>Yu. A. Bychkov, S. V. Iordanskii, and G. M. Eliashberg, *Pis'ma Zh. Eksp. Teor. Fiz.* **33**, 152 (1981) [*JETP Lett.* **33**, 143 (1981)].
- <sup>18</sup>C. Kallin and B. I. Halperin, *Phys. Rev. B* **30**, 5655 (1984).
- <sup>19</sup>Y. E. Lozovik, I. V. Ovchinnikov, S. Y. Volkov, L. V. Butov, and D. S. Chemla, *Phys. Rev. B* **65**, 235304 (2002).
- <sup>20</sup>I. Bar-Joseph, *Semicond. Sci. Technol.* **20**, R29 (2005).
- <sup>21</sup>F. M. Peeters, C. Riva, and K. Varga, *Physica B* **300**, 139 (2001).
- <sup>22</sup>A. Wójs and P. Hawrylak, *Phys. Rev. B* **51**, 10880 (1995).
- <sup>23</sup>J. J. Palacios, D. Yoshioka, and A. H. MacDonald, *Phys. Rev. B* **54**, R2296 (1996).
- <sup>24</sup>D. M. Whittaker and A. J. Shields, *Phys. Rev. B* **56**, 15185 (1997).
- <sup>25</sup>M. Hayne, C. L. Jones, R. Bogaerts, C. Riva, A. Usher, F. M. Peeters, F. Herlach, V. V. Moshchalkov, and M. Henini, *Phys. Rev. B* **59**, 2927 (1999).
- <sup>26</sup>F. M. Munteanu, Y. Kim, C. H. Perry, D. G. Rickel, J. A. Simmons, and J. L. Reno, *Phys. Rev. B* **61**, 4731 (2000); F. M. Munteanu, D. G. Rickel, C. H. Perry, Y. Kim, J. A. Simmons, and J. L. Reno, *ibid.* **62**, 16835 (2000).
- <sup>27</sup>G. Yusa, H. Shtrikman, and I. Bar-Joseph, *Phys. Rev. Lett.* **87**, 216402 (2001).
- <sup>28</sup>T. Vanhouscke, M. Hayne, M. Henini, and V. V. Moshchalkov, *Phys. Rev. B* **63**, 125331 (2001); **65**, 041307 (2002); **65**, 233305 (2002); M. Hayne, T. Vanhouscke, and V. V. Moshchalkov, *ibid.* **68**, 035322 (2003).
- <sup>29</sup>G. V. Astakhov, D. R. Yakovlev, V. V. Rudenkov, P. C. M. Christianen, T. Barrick, S. A. Crooker, A. B. Dzyubenko, W. Ossau, J. C. Maan, G. Karczewski, and T. Wojtowicz, *Phys. Rev. B* **71**, 201312(R) (2005).
- <sup>30</sup>A. Wójs, J. J. Quinn, and P. Hawrylak, *Phys. Rev. B* **62**, 4630 (2000).
- <sup>31</sup>C. Riva, F. M. Peeters, and K. Varga, *Phys. Rev. B* **61**, 13873 (2000); **63**, 115302 (2001); **64**, 235301 (2001).
- <sup>32</sup>D. Andronikov, V. Kochereshko, A. Platonov, T. Barrick, S. A. Crooker, and G. Karczewski, *Phys. Rev. B* **72**, 165339 (2005).
- <sup>33</sup>J. E. Avron, I. W. Herbst, and B. Simon, *Ann. Phys. (N.Y.)* **114**, 431 (1978).
- <sup>34</sup>A. B. Dzyubenko and A. Y. Sivachenko, *Phys. Rev. Lett.* **84**, 4429 (2000); A. B. Dzyubenko, *Solid State Commun.* **113**, 683 (2000).
- <sup>35</sup>I. V. Lerner and Yu. E. Lozovik, *Zh. Eksp. Teor. Fiz.* **80**, 1488 (1981) [*Sov. Phys. JETP* **53**, 763 (1981)].
- <sup>36</sup>A. B. Dzyubenko and Yu. E. Lozovik, *Fiz. Tverd. Tela (Leningrad)* **25**, 1519 (1983) [*Sov. Phys. Solid State* **25**, 874 (1983)].
- <sup>37</sup>A. H. MacDonald and E. H. Rezayi, *Phys. Rev. B* **42**, 3224 (1990).
- <sup>38</sup>C. Schüller, K.-B. Broocks, Ch. Heyn, and D. Heitmann, *Phys. Rev. B* **65**, 081301(R) (2002).
- <sup>39</sup>C. R. L. P. N. Jeukens, P. C. M. Christianen, J. C. Maan, D. R. Yakovlev, W. Ossau, V. P. Kochereshko, T. Wojtowicz, G. Karczewski, and J. Kossut, *Phys. Rev. B* **66**, 235318 (2002).
- <sup>40</sup>P. Plochocka, P. Kossacki, W. Maslana, J. Cibert, S. Tatarenko, C. Radzewicz, and J. A. Gaj, *Phys. Rev. Lett.* **92**, 177402 (2004).
- <sup>41</sup>B. Stebe, E. Feddi, A. Ainane, and F. Dujardin, *Phys. Rev. B* **58**, 9926 (1998).
- <sup>42</sup>R. B. Laughlin, *Phys. Rev. Lett.* **50**, 1395 (1983).
- <sup>43</sup>A. Wójs, P. Hawrylak, and J. J. Quinn, *Phys. Rev. B* **60**, 11661 (1999); A. Wójs, I. Szlufarska, K.-S. Yi, and J. J. Quinn, *ibid.* **60**, R11273 (1999).
- <sup>44</sup>D. Sanvitto, D. M. Whittaker, A. J. Shields, M. Y. Simmons, D. A. Ritchie, and M. Pepper, *Phys. Rev. Lett.* **89**, 246805 (2002).
- <sup>45</sup>T. T. Wu and C. N. Yang, *Nucl. Phys. B* **107**, 365 (1976).
- <sup>46</sup>F. D. M. Haldane, *Phys. Rev. Lett.* **51**, 605 (1983).
- <sup>47</sup>B. E. Cole, J. M. Chamberlain, M. Henini, T. Cheng, W. Batty, A. Wittlin, J. A. A. J. Perenboom, A. Ardavan, A. Polisski, and J. Singleton, *Phys. Rev. B* **55**, 2503 (1997).
- <sup>48</sup>I.-H. Tan, G. L. Snider, L. D. Chang, and E. L. Hu, *J. Appl. Phys.* **68**, 4071 (1990).
- <sup>49</sup>G. Finkelstein, H. Shtrikman, and I. Bar-Joseph, *Phys. Rev. B* **53**, 12593 (1996).
- <sup>50</sup>A. B. Dzyubenko, *Phys. Rev. B* **69**, 115332 (2004).
- <sup>51</sup>A. Wójs, L. Bryja, J. Misiewicz, M. Potemski, D. Reuter, and A. Wieck, in *Proceedings of the XXXV International School on the Physics of Semiconducting Compounds "Jaszowiec 2006," Ustroń, Poland, 2006* [*Acta Phys. Pol. A* (to be published)].